PAPER • OPEN ACCESS

The role of collisionless trapped electron mode turbulence on removal of helium ash and transport of deuterium-tritium ions

OPEN ACCESS
IOP Publishing | International Atomic Energy Agency
Nuclear Fusion
Nucl. Fusion **61** (2021) 016020 (12pp)
https://doi.org/10.1088/1741-4326/abc080

The role of collisionless trapped electron mode turbulence on removal of helium ash and transport of deuterium-tritium ions

Weixin Guo[1], Mingzhu Zhang[1,2], Lu Wang[1,a] and Ge Zhuang[3]

[1] International Joint Research Laboratory of Magnetic Confinement Fusion and Plasma Physics, State Key Laboratory of Advanced Electromagnetic Engineering and Technology, School of Electric and Electronic Engineering, Huazhong University of Science and Technology, Wuhan 430074, China
[2] School of Physics, Huazhong University of Science and Technology, Wuhan 430074, China
[3] Department of Engineering and Applied Physics School of Physical Sciences, University of Science and Technology of China, Hefei 230026, China

E-mail: luwang@hust.edu.cn

Received 9 June 2020, revised 19 September 2020
Accepted for publication 13 October 2020
Published 30 November 2020

Abstract

Removal of helium ash and the anomalous transport of deuterium (D) and tritium (T) ions driven by collisionless trapped electron mode (CTEM) turbulence in tokamak plasmas with weak magnetic shear are studied. We derive the eigenvalue of CTEM with helium ash, and calculate the quasi-linear turbulent fluxes of helium ash, D and T ions simultaneously. Based on the analytical results, the parametric dependence of CTEM instability as well as the anomalous transport of helium ash and D-T ions is investigated, in order to explore the parameter region that is favorable for expelling more helium ash than D and T ions. It is found that helium ash with higher temperature and steeper density profile plays a role of destabilizing CTEM instability, and has higher transport level than that of T ions. We also find that increasing electron temperature and flattening electron density profile are favorable for exhausting helium ash. Isotopic effects (i.e. increasing the fraction of T ions) enhance the transport of both helium ash and D-T ions. Moreover, the trend of stronger transport level of helium ash than that of D-T ions is enhanced by raising electron temperature and flattening electron density profile as well as isotopic effects. Besides, the diffusivity is much larger than the convection. This indicates that the CTEM turbulence driven helium ash transport is favorable for removing helium ash under the parameter region used in the present paper. The possible relevance of our theoretical results to experimental observations is also discussed.

Keywords: helium ash removal, D-T ions, CTEM turbulence, isotopic effects, tokamak plasmas

(Some figures may appear in colour only in the online journal)

1. Introduction

Helium ash is an unavoidable impurity component in the deuterium (D)-tritium (T) plasmas. The accumulation of helium ash in the core will dilute the fuels and cool the plasmas resulting in the decrease of fusion power, and is unfavorable for the success of ignition. Therefore, removing helium

[a] Author to whom any correspondence should be addressed.

ash from the core plasmas and controlling the concentration of helium ash in the core are necessary on the path towards successful achievement of economic fusion power production. For example, the International Thermonuclear Experimental Reactor (ITER) requires the concentration of helium ash should not exceed 10% [1]. Previous studies have pointed out efficiency of exhausting helium ash depends on not only the recycling and pumping in the plasmas edge but also the intrinsic transport of helium from the core to the edge [2–4]. In this regard, understanding the transport of helium ash [5–8] has been treated as one of the most crucial issues for fusion burning plasmas.

The transport of helium impurity has been extensively studied by external helium puffing or beam injection. The corresponding experimental results such as on PDX [9], TFTR [10, 11], TEXTOR [12], DIII-D [13], JT-60U [14] and JET [4] clearly show the transport of helium is anomalous, which is caused by drift wave turbulence [15]. Up to now, only JET and TFTR have ever run the D-T experiments, and the transport of helium ash was also found to be anomalous in TFTR except in the very central region [16], where neoclassical transport might be dominant mechanism. Therefore, it is meaningful to study the anomalous transport of helium ash driven by drift wave turbulence.

Both the simulation [17] and our previous theoretical work [18] based on gyro-kinetic theory revealed that the ion temperature gradient (ITG) mode turbulence is helpful for expelling the helium ash. Recently, we also studied the transport of helium ash driven by parallel velocity shear (PVS) turbulence [19], which is developed from PVS driven Kelvin–Helmholtz instability [20, 21]. However, collisionless trapped electron mode (CTEM) turbulence driven by the trapped electron precession drift resonance [22] could be also an important potential contributor to the anomalous transport of helium ash in fusion devices. It has been observed that CTEM turbulence is the dominant mechanism for the anomalous helium transport in MAST [23]. But, to our knowledge, the anomalous transport of helium ash driven by CTEM turbulence has not been theoretically studied. It is worth to note that dominant electron heating was found to be favorable for removing impurity, especially for low-Z impurities [24]. Here, Z is the charge number of impurity. So, it is also interesting to investigate the following questions: whether helium ash can be removed through CTEM turbulence? How is the parametric dependence of the transport of helium ash in D-T plasmas?

Moreover, most of existing works focus only on the anomalous transport of helium ash [18, 19], and few works care the transport of both impurity and main ions simultaneously. Recent experimental results on Large Helical Device (LHD) studied the transport of carbon and hydrogen (H)-D ions, separately [25]. One may wonder whether the transport of helium ash is different from D-T ions or not. Indeed, during D-T operation on TFTR, it is found that the diffusivities of T ions and helium ash are similar in magnitude, but the convective velocities of them are different [26]. It would be great to find parameter regime to expel more helium ash than D-T ions. Thus, studying the anomalous transport of both helium ash and D-T ions driven by CTEM turbulence simultaneously is of great significance for future burning plasmas.

At the same time, understanding the isotopic effects (i.e. the effects of varying the effective mass number of hydrogen isotopes) on confinement and anomalous transport is a long-standing issue for the research of magnetic confinement fusion. Recently, this topic has attracted a lot of attention [27–35] due to the operation of D plasmas on LHD [36, 37] and approaching to the JET-DTE2 [38]. The gyro-kinetic simulations by GKV verified the universal nature of isotopic effects on trapped electron mode (TEM) turbulence in both axisymmetric tokamaks and non-axisymmetric helical/stellarator systems [33, 39]. The presence of impurity can modify the isotopic dependence of TEM instability [40]. But, the isotopic effects on helium ash transport driven by CTEM turbulence are still an indistinct issue.

In this paper, we will focus on the anomalous transport of helium ash and D-T ions induced by electron density gradient driven CTEM turbulence in tokamak plasmas, and try to elucidate the favorable parameter regime for expelling more helium ash than D-T ions. Although electron temperature gradient can be also the drive of CTEM turbulence, this is not the focus of this work. We firstly derive the eigenmode equation of CTEM instability in D-T plasmas with helium ash based on the gyro-kinetic and bounce-kinetic theories, and then study the parametric dependence of CTEM instability. For simplicity, the equilibrium distribution function for both helium ash and D-T ions are assumed to be Maxwellian. The temperature of helium ash used in this work is a free parameter, which could be slightly higher or lower than that of background plasmas. More importantly, we derive the quasi-linear fluxes of helium ash, D and T ions simultaneously, and study the parametric dependence of the transport of both helium ash and D-T ions based on the analytical results. The isotopic dependence of CTEM instability and particle transport is also discussed. However, the isotopic effects on collisions [33], bounce-kinetic equation [34], zonal flow [35] as well as the combination of isotopic effects and electromagnetic effects [31, 32] are beyond the scope of this paper. The **principal results** can be summarized as:

(a) Higher (Lower) temperature of helium ash destabilizes (stabilizes) the CTEM instability, and steeper density profile of helium ash can further enhance this trend. The critical temperature ratio between electrons and helium ash for distinguishing the role of destabilization and stabilization by helium ash is given. Besides, it is relatively easier to expel helium ash when its temperature is slightly higher than that of background plasmas ($T_e = T_i < T_z$).

(b) Increasing electron temperature ($T_e > T_i = T_z$) and flattening electron density profile not only destabilize the CTEM instability with helium ash but also enhance the transport level of both helium ash and D-T ions. Moreover, the higher electron temperature and the flatter electron density profile we have, the easier to expel more helium ash than D-T ions it is.

(c) Isotopic effects enhance the transport level of both helium ash and D-T ions and the trend of stronger transport level of helium ash than that of D-T ions.
(d) Under the parameters used in the present paper, the CTEM driven diffusion dominants over convection, which is favorable for expelling helium ash.

The remainder of this paper is organized as follows. In section 2, we will present the derivation of eigenmode equation and its solution, and explore how some key parameters affect CTEM instability in D-T plasmas with helium ash. In section 3, the quasi-linear fluxes and the corresponding transport coefficients (i.e. diffusivity and convective velocity) of helium ash, D and T ions are calculated simultaneously. Then, the parametric dependence (such as the temperature of helium ash, the density gradient of helium ash, the electron temperature, the electron density gradient and isotope fuel mixing ratio) of the anomalous transport of helium ash, D and T ions driven by CTEM turbulence will be studied in detail. Finally, summary and some related discussions are given in section 4.

2. CTEM instability in D-T plasmas with helium ash

In this section, we will derive the eigenmode equation for CTEM instability by employing gyro-kinetic (bounce-kinetic) theory for helium ash, D and T ions (electrons). After solving the eigenmode equation and getting the real frequency and linear growth rate in section 2.1, we mainly analyze the parametric dependence of CTEM instability with helium ash in section 2.2.

2.1. The eigenmode equation and its solutions for CTEM instability

Similar to the ITG and PVS instability [18, 19], we deal with helium ash, D and T ions by gyro-kinetic theory. The equilibrium distribution function for both helium ash and D-T ions are assumed to be Maxwellian. We choose the sheared slab geometry with $\vec{B}=B\left(\vec{e}_z+\frac{x}{L_s}\vec{e}_y\right)$, where x, y and z correspond to the coordinates of radial, poloidal and toroidal in the tokamak configuration, respectively, B is the magnetic field along z direction, and $L_s=qR/\hat{s}$ means the scale length of magnetic shear (R is the major radius, q is the safety factor, $\hat{s}$ is the magnetic shear). After linearizing gyrocenter Vlasov equation and pull-back transformation, the perturbed density of species α ($\alpha=z$, D, T represents the helium ash, D and T ions, respectively) can be given by

$$\delta n_{\alpha,k}=-\left\{\frac{\omega_{*\alpha}}{\omega}+\left[1-\frac{\omega_{*\alpha}}{\omega}(1+\eta_\alpha)\right]\left[b_\alpha-\rho_\alpha^2\frac{\partial^2}{\partial x^2}-\left(\frac{k'_{||}v_{th\alpha}}{\omega}\right)^2x^2\right]\right\}\frac{Z_\alpha e\delta\phi_k(x)}{T_\alpha}n_{0\alpha}. \tag{1}$$

Here, the first term in the bracket is called 'hydromagnetic' term, while the second term corresponds to the modifications due to *both* finite Larmor radius (FLR) effects *and* acoustic term. $k_\perp^2$ is treated as $k_\perp^2=k_y^2-\frac{\partial^2}{\partial x^2}$ with k_y being the poloidal wavenumber. Therefore, the FLR effects include both $b_\alpha=k_y^2\rho_\alpha^2$ and $\rho_\alpha^2\frac{\partial^2}{\partial x^2}$ terms which correspond to y and x directions, and $\rho_\alpha=\frac{v_{th\alpha}}{\Omega_\alpha}$ is the gyroradius with $v_{th\alpha}=\sqrt{\frac{T_\alpha}{m_\alpha}}$ and $\Omega_\alpha=\frac{Z_\alpha eB}{cm_\alpha}$ being the thermal velocity and gyrofrequency, T_α and m_α being the temperature and mass of species α. The acoustic term is proportional to $\left(\frac{k'_{||}v_{th\alpha}}{\omega}\right)^2x^2$, where ω means the frequency of CTEM instability. We have expressed the electrostatic potential in the Fourier space as $\delta\phi\left(\vec{r}\right)=\sum_k\delta\phi_k(x)e^{-i\omega t+ik_yy+ik_{||}z}$ and taken the parallel wavenumber $k_{||}=k'_{||}x$ with $k'_{||}=\frac{k_y}{L_s}$ and x being the distance away from the rational surface. The expressions of the other symbols in equation (1) are: $\omega_{*\alpha}=-\frac{k_y}{L_{n\alpha}}\frac{cT_\alpha}{Z_\alpha eB}$ is the diamagnetic drift frequency, where $L_{n\,\alpha}=-\frac{n_{0\alpha}}{\nabla n_{0\alpha}}$ is the density gradient scale length of species α with $n_{0\alpha}$ being the equilibrium density, Z_α being the charge number ($Z_\alpha=Z$ for helium ash and $Z_\alpha=1$ for D and T ions), c is the light speed in vacuum, e is the elementary charge, and $\eta_\alpha=\frac{L_{n\alpha}}{L_{T\alpha}}$ with $L_{T\alpha}=-\frac{T_\alpha}{\nabla T_\alpha}$ being the temperature gradient scale length of species α.

For electrons, bounce-kinetic theory is utilized to calculate the perturbed density of trapped electrons in the toroidal configuration, and passing electrons is assumed to be adiabatic. Then, the perturbed density of electrons is represented as [22, 41]

$$\delta n_{e,k}=\chi_e\frac{e\delta\phi_k(x)}{T_e}n_{0e}, \tag{2}$$

with the susceptibility of electrons being

$$\chi_e=1-\sqrt{2\varepsilon_0}\left(1-\frac{\omega_{*e}}{\omega}\right)-\frac{3}{2}\sqrt{2\varepsilon_0}\frac{\bar{\omega}_{de}G_{av}}{\omega}\left(1-\frac{\omega_{*e}}{\omega}K_e\right)+i2\sqrt{2\pi\varepsilon_0}\left(\frac{\omega}{\bar{\omega}_{de}G_{av}}\right)^{3/2}\exp\left(-\frac{\omega}{\bar{\omega}_{de}G_{av}}\right)\left\{1-\frac{\omega_{*e}}{\omega}\left[1+\eta_e\left(\frac{\omega}{\bar{\omega}_{de}G_{av}}-\frac{3}{2}\right)\right]\right\}. \tag{3}$$

The first term on the right hand side of equation (3) is contributed by passing electrons, the second and third terms come from the contribution of non-resonant trapped electrons, while the fourth term is from the resonant electrons. Here, $\varepsilon_0=\frac{r}{R}$ is the inverse aspect ratio with r being the minor radius, $\omega_{*e}=\frac{k_y}{L_{ne}}\frac{cT_e}{eB}$ is the electron diamagnetic drift frequency with $L_{ne}=-\frac{n_{0e}}{\nabla n_{0e}}$ representing the electron density gradient scale length and n_{0e} being the equilibrium electron density, $\bar{\omega}_{de}=\frac{L_{ne}}{R}\omega_{*e}$ means the bounce averaged magnetic drift frequency of trapped electrons, $G_{av}=0.64\hat{s}+0.57$ is obtained by averaging over the azimuthal angle of the turning point of a trapped electron [42], $K_e=1+\eta_e$, $\eta_e=\frac{L_{ne}}{L_{Te}}$ and $L_{Te}=-\frac{T_e}{\nabla T_e}$ is the electron temperature gradient scale length with T_e being the electron temperature.

Then, bringing equations (1) and (2) into the quasi-neutrality equation, we can get the differential eigenmode equation of CTEM instability and it is a Weber equation expressed as

$$\left(A_W\frac{\partial^2}{\partial\bar{x}^2}+B_W-C_W\bar{x}^2\right)\delta\phi_k(\bar{x})=0. \tag{4}$$

Here, $\bar{x}=x/\rho_H$, $A_W=-\tau_H\tilde{f}_z\left(1+C_1\frac{1}{\hat{\omega}}\bar{K}\right)$, $B_W=\chi_e-C_1\frac{1}{\hat{\omega}}+\tau_H b_H\tilde{f}_z\left(1+C_1\frac{1}{\hat{\omega}}\bar{K}\right)$, $C_W=\tau_H b_H S^2\frac{1}{\hat{\omega}^3}l_0^2F^2(\hat{\omega})\tilde{f}_z(\hat{\omega}+C_1\bar{K})$, $C_1=\tau_H k_y\rho_H\frac{R}{L_{ne}}$, $\tau_H=\frac{T_e}{T_H}$ is the temperature ratio between electrons and H ions, $\tilde{f}_z=(1-Zf_c)A_{i,\,eff}+f_cA_z$ with $A_{i,eff}=f_DA_D+f_TA_T$ being the effective ion mass. $f_D=n_{0D}/(n_{0D}+n_{0T})$ and $f_T=1-f_D$ are the fractions of D ions and T ions, respectively, and the larger f_T, the larger $A_{i,eff}$. $f_c=n_{0z}/n_{0e}$ is the concentration of helium ash, A_α is the mass number of species α ($A_z=4$ for helium ash, $A_D=2$ for D ions and $A_T=3$ for T ions), $l_0=\sqrt{\frac{1}{A_{\mathrm{i,\,eff}}}\left(\frac{f_D}{A_D}+\frac{f_T}{A_T}\right)}$, $\hat{\omega}=\frac{\omega}{v_{thH}/R}$ corresponds to the normalized frequency of CTEM instability, $\bar{K}=\frac{(1-Zf_c)(f_DA_DL_{eD}K_D+f_TA_TL_{eT}K_T)+f_c\frac{A_z}{Z}L_{ez}K_z}{\tilde{f}_z}$ is the effective ion temperature gradient with $L_{e\alpha}=L_{ne}/L_{n\alpha}$ being the dimensionless density gradient scale length ratio, $K_\alpha=(1+\eta_\alpha)/\tau_\alpha$ with $\tau_\alpha=T_e/T_\alpha$ being the temperature ratio between electrons and species α, $b_{\mathrm{H}}=k_y^2\rho_{\mathrm{H}}^2$, $S=R/L_s$. $(1-Zf_c)(f_DL_{eD}+f_TL_{eT})+Zf_cL_{ez}=1$ is satisfied due to the quasi-neutrality condition of equilibrium densities. Moreover, we know that the solution of a Weber equation is Hermite function, i.e. the ℓth order $\delta\phi_k(\bar{x})^{(\ell)}=H_\ell(\sqrt{\sigma}\bar{x})e^{-\sigma\bar{x}^2/2}$ where H_ℓ is the Hermite polynomial and $\sigma=\sqrt{C_W/A_W}=ik_y\rho_HS\frac{1}{\hat{\omega}}l_0F(\hat{\omega})$. Here, the positive sign for σ is adopted due to the condition of waves with outgoing energy flux. $F(\hat{\omega})=\sqrt{1+f_c\frac{A_z\left(\frac{Z^2}{A_z^2}-l_0^2\right)\left(1+\frac{C_1}{\hat{\omega}}\frac{L_{ez}}{Z}K_z\right)}{l_0^2\tilde{f}_z\left(1+\frac{C_1}{\hat{\omega}}\bar{K}\right)}}$ due to the hypothesis of $L_{nD}=L_{nT}$ and $T_D=T_T$ (thus $L_{eD}=L_{eT}$ and $K_D=K_T$) used in this work. We can clearly see that $F(\hat{\omega})\approx1$ when the concentration of helium ash f_c is small. Thus, we will use the simplification $F(\hat{\omega})\approx1$ in the following calculation in order to get analytical progresses. It should be noted that equation (4) is exactly the same as equation (7) of [19]. if we ignore the non-adiabatic electrons and PVS effects. However, we normalize the distance away from rational surface x by ρ_H and the frequency by v_{thH}/R in this work rather than by ion acoustic Larmor radius ρ_s and ω_{*e} as in [19]. This will be helpful for the analysis of parametric dependence of our results, since the effects of electron temperature, electron density gradient and effective ion mass number on the normalization are eliminated. Finally, the dispersion relation of CTEM instability in the presence of helium ash can be determined by solving equation (4),

$$\begin{aligned}&\left(1-\sqrt{2\varepsilon_0}+\tau_Hb_H\tilde{f}_z\right)\hat{\omega}^2+\left[\sqrt{2\varepsilon_0}\left(C_1-\frac{3}{2}\tau_Hk_y\rho_HG_{av}\right)\right.\\&\left.-C_1+C_1\tau_Hb_H\tilde{f}_z\bar{K}+i\tau_Hk_y\rho_HSl_0\tilde{f}_z\right]\hat{\omega}\\&+\frac{3}{2}\sqrt{2\varepsilon_0}\tau_Hk_y\rho_HC_1G_{av}(1+\eta_e)+i\tau_Hk_y\rho_HSl_0\tilde{f}_zC_1\bar{K}\\&+i2\sqrt{2\pi\varepsilon_0}\left(\frac{\hat{\omega}}{G_{av}\tau_Hk_y\rho_H}\right)^{3/2}\exp\left(-\frac{\hat{\omega}}{G_{av}\tau_Hk_y\rho_H}\right)\\&\times\left[\hat{\omega}\left(1-\frac{R/L_{Te}}{G_{av}}\right)+C_1\left(\frac{3}{2}\eta_e-1\right)\right]\hat{\omega}=0,\end{aligned} \tag{5}$$

where $\ell=0$ has been chosen. If we further express the normalized eigenvalue $\hat{\omega}=\hat{\omega}_r+i\hat{\gamma}_k$ ($\hat{\omega}_r=\frac{\omega_r}{v_{thH}/R}$, $\hat{\gamma}_k=\frac{\gamma_k}{v_{thH}/R}$ with $\hat{\gamma}_k\ll\hat{\omega}_r$) and assume the ordering of $S\sim b_H\sim\frac{\hat{\gamma}_k}{\hat{\omega}_r}\sim\frac{\bar{\omega}_{de}}{\omega_{*e}}\sim\varepsilon_0$, the normalized real frequency and growth rate of CTEM instability in the plasmas with helium ash are calculated by neglecting the higher order terms,

$$\hat{\omega}_r=C_1\frac{1-\tau_Hb_H\tilde{f}_z\bar{K}-\sqrt{2\varepsilon_0}\left(1+\frac{3}{2}\frac{G_{av}}{R/L_{ne}}\eta_e\right)}{1-\sqrt{2\varepsilon_0}+\tilde{f}_z\tau_Hb_H}, \tag{6}$$

$$\hat{\gamma}_k=\frac{2\sqrt{2\pi\varepsilon_0}\left(\frac{\hat{\omega}_r}{G_{av}\tau_Hk_y\rho_H}\right)^{3/2}\exp\left(-\frac{\hat{\omega}_r}{G_{av}\tau_Hk_y\rho_H}\right)\left[\hat{\omega}_r\left(\frac{R}{L_{Te}G_{av}}-1\right)+C_1\left(1-\frac{3}{2}\eta_e\right)\right]\hat{\omega}_r-\tau_Hk_y\rho_HSl_0\tilde{f}_z(C_1\bar{K}+\hat{\omega}_r)}{C_1\left[1-\sqrt{2\varepsilon_0}\left(1-\frac{3}{2}\frac{G_{av}}{R/L_{ne}}\right)-\tau_Hb_H\tilde{f}_z\bar{K}\right]-3\sqrt{2\varepsilon_0}\tau_Hk_y\rho_HG_{av}K_e}. \tag{7}$$

Equation (6) clearly shows that FLR effects can cause the downshift of real frequency, which is consistent with the case without helium ash. This downshift of real frequency destabilizes CTEM instability. In particular, the scale length of helium ash density gradient (i.e. $\frac{R}{L_{n\,z}}=L_{e\,z}\frac{R}{L_{n\,e}}$) as well as the temperature of helium ash (i.e. τ_z with fixed T_e) can also affect the real frequency via influence on $\tilde{f}_z\bar{K}$, and thus affect CTEM instability. Since we have used the hypothesis of $L_{n\,D}=L_{n\,T}$ and $T_D=T_T$, $\tilde{f}_z\bar{K}$ can be rewritten as

$$\tilde{f}_z\bar{K}=\frac{A_{i,eff}}{\tau_i}\left(1+\frac{L_{n\,e}}{L_{T\,z}}\right)+Zf_c\left(\frac{R}{L_{n\,z}}+\frac{R}{L_{T\,z}}\right)\frac{L_{n\,e}}{R}\left(\frac{A_z}{Z^2\tau_z}-\frac{A_{i,eff}}{\tau_i}\right). \tag{8}$$

Here, τ_i ($i=D,\,T$) is temperature ratio between electrons and ions, and $\tau_D=\tau_T=\tau_H=\tau_i$ is used in the present work.

It is worth to note that the $\frac{A_z}{Z^2\tau_z} - \frac{A_{i,eff}}{\tau_i}$ term is directly proportional to $\rho_z^2 - \rho_{i,\,eff}^2$, where $\rho_{i,\,eff}$ is the effective ion gyroradius defined by $A_{i,eff}$. In addition, $L_{n\,z}$, $L_{n\,e}$ and $L_{T\,z}$ are all positive in equation (8) in our work, and the stronger FLR effects for $\rho_z > (<)\,\rho_{i,\,eff}$ destabilize (stabilize) CTEM instability due to the presence of helium ash. Thus, we can immediately identify a critical value of τ_z determined by $\frac{A_z}{Z^2\tau_z} - \frac{A_{i,eff}}{\tau_i}$=0 for distinguishing the destabilization and stabilization role of the presence of helium ash,

$$\tau_{z,\,cri} = \tau_i \frac{A_z}{Z^2 A_{i,eff}}. \tag{9}$$

Moreover, steeper helium ash density profile, i.e. larger R/L_{nz} can further stabilize (destabilize) the CTEM instability more for τ_z> (<) $\tau_{z,\,cri}$.

From equations (6) and (7), we can also analyze the effects of the other parameters on CTEM instability, which will be shown soon. For example, how electron temperature and electron density gradient affect the CTEM instability with helium ash? This might be relevant to the effects of electron cyclotron resonance heating (ECRH) on the anomalous transport of 'non-trace' helium ash. Here, 'non-trace' means the concentration helium ash is not ignorable, and the presence of helium ash affects the micro-instabilities [43]. Meanwhile, isotopic effects can be analyzed by varying the fraction of T ions (i.e. f_T). More results can be found in section 2.2.

2.2. Parametric dependence of CTEM instability with helium ash

In this subsection, we will investigate the parametric dependence of CTEM instability in the D-T plasmas with helium ash in detail. Unless otherwise stated, we set the parameters as: the fuel ratio of D-T mixing plasmas is 1:1, $k_y\rho_H = 0.3$, τ_i =1, ε_0= 0.1, q = 1.5 and relative weak magnetic shear $\hat{s}$ = 0.1, f_c = 10%, τ_z = 1, $\frac{R}{L_{Ti}} = \frac{R}{L_{Tz}}$ = 0.1, $\frac{R}{L_{Te}}$ = 0.1, $\frac{R}{L_{ne}}$ = 5 and $\frac{R}{L_{nz}}$ = 10 (i.e. L_{ez}=2).

2.2.1. $k_y\rho_H$ spectrum. Firstly, the wave number spectrum of eigenvalue is shown in figure 1. The normalized real frequency $\hat{\omega}_r$ does not change significantly with the initial increase of $k_y\rho_H$ due to the competition between the increased coefficient C_1 and the downshift by FLR effects. While, with further increase of $k_y\rho_H$, the downshift of the normalized real frequency dominates, and the CTEM instability is destabilized synchronously. This is because lower real frequency makes more electrons resonate with the waves and thus increases the growth rate. The monotonic increase of CTEM instability with wave number is also found in [44]. Besides, the different lines in figure 1(*b*) also indicate that helium ash with $T_z = T_i = T_e$ stabilizes the CTEM instability. As mentioned in the introduction, the temperature of helium ash could be slightly lower or higher than that of background ions. This may result in different effects of helium ash on CTEM instability.

2.2.2. Effects of T_z and R/L_{nz}. In figure 2, we plot the variation of $\hat{\omega}_r$ and $\hat{\gamma}_k$ as a function of τ_z. It needs to be

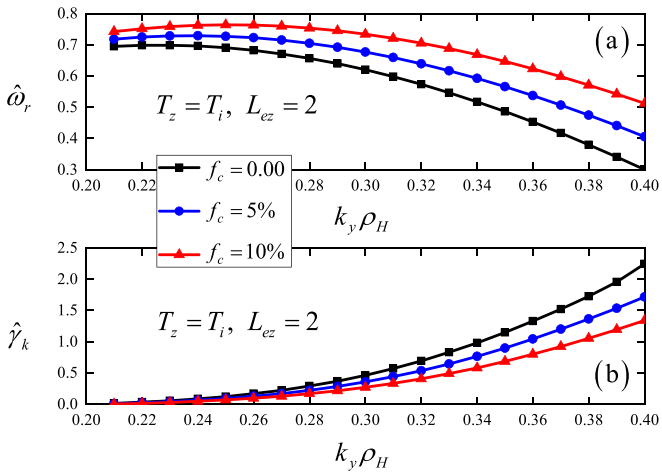

Figure 1. Normalized real frequency $\hat{\omega}_r$ (*a*) and growth rate $\hat{\gamma}_k$ (*b*) as a function of $k_y\rho_H$ for different concentration of helium ash.

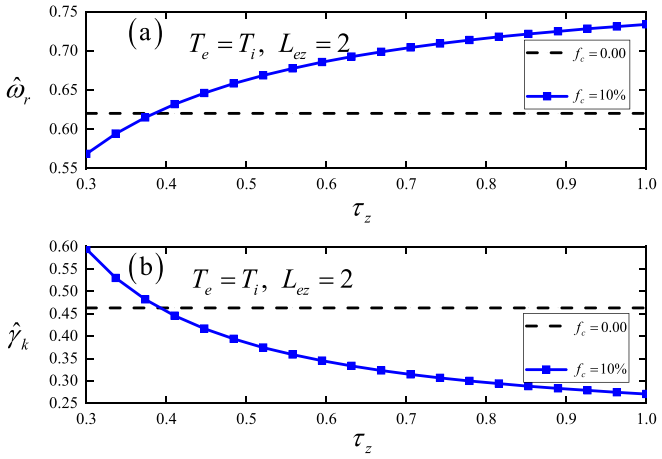

Figure 2. Normalized real frequency $\hat{\omega}_r$ (*a*) and growth rate $\hat{\gamma}_k$ (*b*) as a function of τ_z with (blue line with square) and without (dashed black line) helium ash in 1:1 D-T plasmas. Varying τ_z here actually means variation of T_z with fixed $T_e = T_i$.

stressed that varying τ_z here actually means variation of T_z with fixed $T_e = T_i$. With the increase of τ_z, it clearly shows that $\hat{\omega}_r$ increases, while synchronously $\hat{\gamma}_k$ decreases. Moreover, as compared to the case without helium ash (f_c = 0), the presence of higher (lower) temperature of helium ash, i.e. smaller (greater) τ_z destabilizes (stabilizes) CTEM instability. Equation (9) gives the critical value of τ_z for distinguishing the role of destabilization and stabilization $\tau_{z,\,cri}$=0.4 for 1:1 D-T plasmas with helium ash, which is consistent with the results in figure 2.

As noted in [45–47], the density profile of impurity can also significantly influence the TEM instability. Different from other types of impurity, the source of helium ash is from the core plasmas, thus its density profile can be only inwardly peaked (R/L_{nz}>0). In figure 3, we illustrate the effects of density profile of helium ash R/L_{nz} on CTEM instability for different τ_z. $\hat{\gamma}_k$ in figure 3(*b*) is increased (decreased) with steepening of helium ash density profile when τ_z< (>) 0.4. The critical value of τ_z for distinguishing the destabilization/stabilization

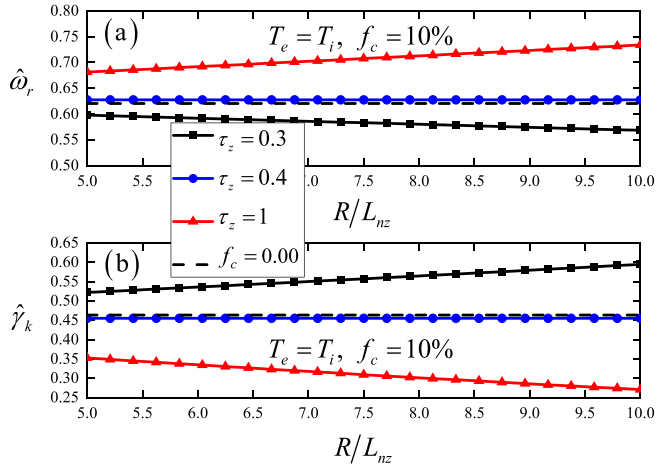

Figure 3. Normalized real frequency $\hat{\omega}_r$ (*a*) and growth rate $\hat{\gamma}_k$ (*b*) as a function of R/L_{nz} in 1:1 D-T plasmas. The dashed black line is the case without helium ash. Variation of τ_z for different lines actually represents the variation of T_z due to fixed T_e=T_i.

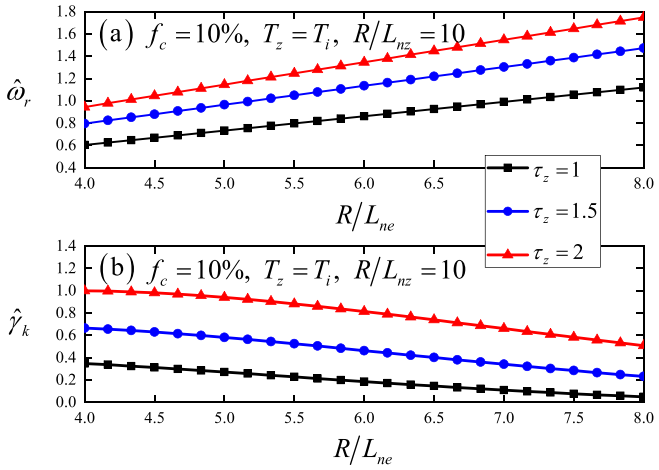

Figure 4. Normalized real frequency $\hat{\omega}_r$ (*a*) and growth rate $\hat{\gamma}_k$ (*b*) vs R/L_{ne} in 1:1 D-T plasmas with 10% helium ash. The different lines for different τ_z actually represent the variation of T_e due to fixed T_i=T_z.

role of R/L_{nz} is also determined by $\tau_{z,\,cri} = \tau_i \frac{A_z}{Z^2 A_{i,eff}}$ as elaborated in equation (9). Here, we notice that the decrease of $\hat{\gamma}_k$ by steepening the density profile of helium ash with τ_z=1 is qualitatively consistent with the result in [45]. with low-Z carbon, but not consistent with that in [48]. with heavy impurity.

2.2.3. Effects of T_e and R/L_{ne}. ECRH effects on impurity transport are widely observed in recent years [14, 49–53]. The electron density profile with additional ECRH in the core can be either flattened [14] or steepened [53, 54]. Motivated by these experimental observations, we study the effects of T_e as well as R/L_{ne} on CTEM instability with helium ash in the following.

In figure 4, the concentration of helium ash in 1:1 D-T plasmas is set to be 10%, and we fix T_i=T_z and $R/L_{nz} = 10$. Thus, varying τ_z actually means the variation of T_e. For fixed R/L_{ne}, we can see that increasing T_e (i.e. increasing τ_z) upshifts the normalized real frequency and destabilizes the CTEM instability with helium ash. This seems different from the analysis in previous subsection where electron temperature is fixed. This is because the upshift of real frequency by increasing T_e is not as strong as that of precession drift frequency due to FLR effects on real frequency. Then, increasing T_e results in more rather than less resonant electrons, which destabilizes CTEM instability. Moreover, for fixed τ_z, it exhibits that flattening the electron density profile (decreasing R/L_{ne}) downshifts $\hat{\omega}_r$, but the growth rate $\hat{\gamma}_k$ is clearly increased. The destabilization by flattening electron density profile in this range is qualitatively consistent with the results in [22]. Combining the effects of increasing electron temperature and flattening the electron density profile may destabilize the CTEM instability synergistically.

2.2.4. Isotopic effects In figure 5, we display how isotopic effects influence the CTEM instability by varying the fraction of T ions f_T. It shows that $\hat{\omega}_r$ is decreased but the growth rate $\hat{\gamma}_k$

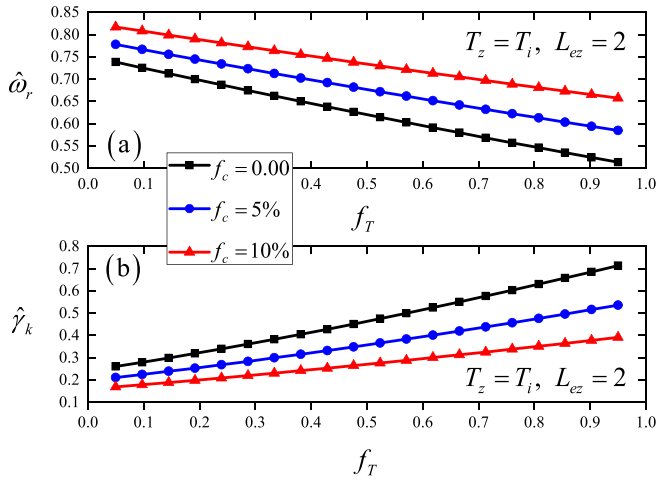

Figure 5. Normalized real frequency $\hat{\omega}_r$ and growth rate $\hat{\gamma}_k$ as a function of the friction of T ions f_T in mixing D-T plasmas with (blue and red lines) and without (black line) helium ash.

is increased when we increase f_T (i.e. increase $A_{i,\,eff}$). This can be also explained by the stronger downshift of real frequency due to the stronger FLR effects for larger $A_{i,\,eff}$ resulting in larger growth rate. Furthermore, the presence of helium ash weakens the destabilization role of isotopic effects on CTEM instability due to its smaller gyroradius as compared to $\rho_{i,\,eff}$, and this trend is enhanced with increasing the concentration of helium ash. However, the destabilization of CTEM instability by isotopic effects (increasing $A_{i,\,eff}$) here is not consistent with figure 1 of [40], where the growth rate of CTEM instability satisfies $\gamma_H > \gamma_D > \gamma_T$ with normal helium impurity (not helium ash) and strong magnetic shear ($\hat{s} = 1.5$). It is also worth noting that the isotopic effects on PVS instability with helium ash were found to be weak [19], and on ITG instability in plasmas with tungsten [55] or carbon [18] is stabilizing. These indicate the isotopic effects on different kinds of micro-instability are different.

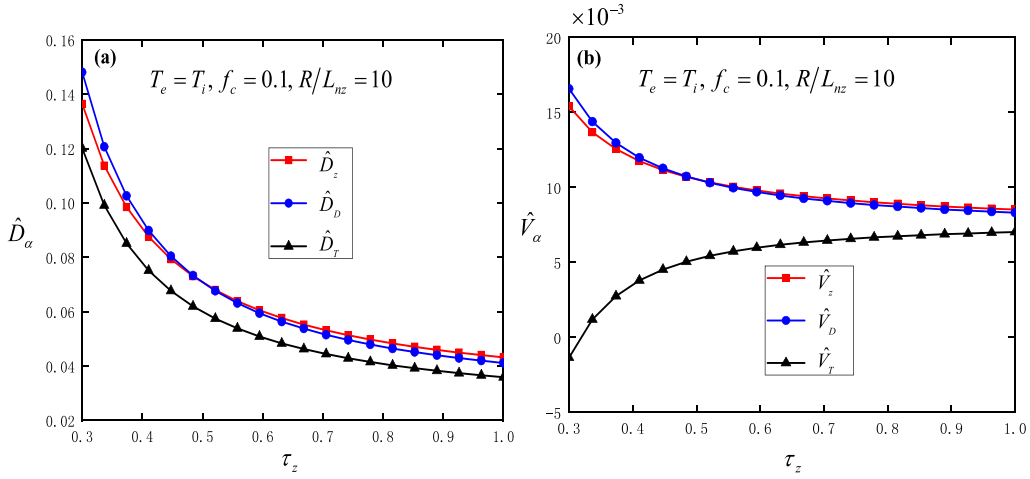

Figure 6. Transport coefficients of helium ash, D and T ions versus temperature ratio between electron and helium ash τ_z. The variation of τ_z here means T_z is varying because of fixed $T_e = T_i$.

3. Anomalous transport of helium ash, D and T ions

In this section, we will firstly derive the quasi-linear fluxes of helium ash as well as D and T ions, and divide the fluxes into diffusive and convective parts. Then, the parametric dependence of anomalous transport of helium ash, D and T ions driven by CTEM turbulence will be analyzed in section 3.2, where we may find the clue about how to expel more helium ash than D and T ions.

3.1. Quasi-linear fluxes and the associated transport coefficients for helium ash, D and T

The quasi-linear turbulent flux of species α ($\alpha = z$, D, T) driven by the radial fluctuating $\vec{E} \times \vec{B}$ drift can be written as

$$\begin{aligned}\Gamma_\alpha &= \mathrm{Re}\left\langle \delta n_\alpha \delta v_{\vec{E}\times\vec{B}} \right\rangle \\ &= -\,\mathrm{Im}\left\langle \sum_k \delta n_{\alpha,k} \frac{ck_y}{B} \delta\phi_k^* \right\rangle. \end{aligned} \tag{10}$$

Here, $\delta\phi_k^*$ is the conjugation component of $\delta\phi_k$. Then, putting the perturbed density of helium ash from equation (1) into equation (10), we get the normalized fluxes of helium ash ($\hat{\Gamma}_z = \frac{\Gamma_z}{n_{0z} v_{thH} \left|\hat{\phi}_k\right|^2}$ with $v_{thH} = \sqrt{\frac{T_H}{m_H}}$ being the thermal velocity of H ions),

$$\hat{\Gamma}_z = (R/L_{nz})\hat{D}_z + \hat{V}_z, \tag{11}$$

where the diffusivity and convective velocity are

$$\hat{D}_z = \sum_k \left(\hat{D}_{z0} + \hat{D}_{z1}\right)(\tau_H k_y \rho_H)^2, \tag{12}$$

and

$$\hat{V}_z = \sum_k \left[\left(\hat{V}_z^{|S|} + \hat{V}_z^{acous}\right) S + \frac{R}{L_{Tz}} \hat{V}_z^{\nabla T_z}\right](\tau_H k_y \rho_H)^2. \tag{13}$$

In equations (12) and (13), we have modelled the averaged square of normalized width of modes around the rational surface as $\left\langle \bar{x}^2 \right\rangle = \left|\frac{L_s}{L_{ne}}\right| = \frac{R}{L_{ne}} \left|\frac{1}{\hat{S}}\right|$, and $\rho_H = \frac{v_{thH}}{\Omega_H}$ with $\Omega_H = \frac{eB}{cm_H}$. Moreover, $\hat{D}_{z0} = \frac{\hat{\gamma}_k}{\hat{\omega}_r^2}$ contributes to the lowest order of diffusivity, $\hat{D}_{z1} = \frac{1}{\hat{\omega}_r^2 \tau_z}\left[\hat{D}_z^{FLR} b_H + \left(\hat{D}_z^{|S|} + \hat{D}_z^{acous}\right)\tau_H k_y \rho_H S\right]$ represents the modification to $\hat{D}_z$ with $\hat{D}_z^{FLR} = -\hat{\gamma}_k \frac{\tau_H A_z}{Z^2}$ and $\hat{D}_z^{|S|} = \frac{A_z}{Z^2} l_0 \left(-l_0 A_z \hat{D}_z^{acous} + 1\right)$ coming from the FLR effects in y and x directions, respectively, and $\hat{D}_z^{acous} = k_y \rho_H \frac{R}{L_{ne}} \frac{3\hat{\gamma}_k}{A_z \hat{\omega}_r^2}$ comes from the impurity acoustic term as expounded in equation (1). Both of the latter two terms are proportional to magnetic shear, and $\left(\hat{D}_z^{|S|} + \hat{D}_z^{acous}\right)\tau_H k_y \rho_H S < -\hat{D}_z^{FLR} b_H$ for weak magnetic shear regime and ∇n_{0e}-driven CTEM instability in the present work. Therefore, the total modification is negative. For the impurity convective velocity $\hat{V}_z$ in equation (13), $\hat{V}_z^{|S|} = \frac{A_z}{Z} l_0 \frac{1}{\hat{\omega}_r}\left(-\frac{2}{3} l_0 A_z \hat{D}_z^{acous} + 1\right)$ comes from the FLR effects in x direction, and can be either inward (<0) or outward (>0), $\hat{V}_z^{acous} = \frac{2Z}{3\hat{\omega}_r} \hat{D}_z^{acous} > 0$ is outward due to impurity acoustic term. It is also needed to note that those two convective terms are linearly proportional to magnetic shear. The coefficient of thermo-diffusion pinch term $\hat{V}_z^{\nabla T_z} = \hat{D}_{z1}$ is inward due to $\hat{D}_{z1} < 0$ for weak magnetic shear regime. Then, the final direction of total convective velocity $\hat{V}_z$ depends on the competition between outward and inward terms.

Similarly, we can also get the anomalous fluxes of D and T ions $\hat{\Gamma}_i = (R/L_{ni})\hat{D}_i + \hat{V}_i$ ($\hat{\Gamma}_i = \frac{\Gamma_i}{n_{0i} v_{thH} \left|\hat{\phi}_k\right|^2}$, $i = D$, T) with the transport coefficients being

$$\hat{D}_i = \sum_k \left(\hat{D}_{i0} + \hat{D}_{i1}\right)(\tau_H k_y \rho_H)^2, \tag{14}$$

$$\hat{V}_i = \sum_k \left[\left(\hat{V}_i^{|S|} + \hat{V}_i^{acous}\right) S + \frac{R}{L_{Ti}} \hat{V}_i^{\nabla T_i}\right](\tau_H k_y \rho_H)^2. \tag{15}$$

For D and T ions, the transport coefficients have the same formation and physical meaning as those for helium ash, thus it would be very easy to get the detailed expressions of every term presented in equations (14) and (15) by replacing A_z by A_i and taking Z=1 in the corresponding terms of equations (12) and (13). So, we do not repeat them here.

The interesting point is that the lowest order of diffusivity $\hat{D}_{\alpha 0}=\frac{\hat{\gamma}_k}{\hat{\omega}_r^2}$ are exactly the same for helium ash and D-T ions. However, the modifications to transport coefficients due to the FLR effects and acoustic terms, which depend on mass number, charge number and temperature of species α, will be different for helium ash and D-T ions. Thus, the total transport coefficients and corresponding turbulent fluxes will be also different for helium ash and D-T ions. In the next part, we will explore the parametric dependence of this difference, and try to identify the parameter regime for higher transport level of helium ash than that of D-T ions.

Before next part, we would like to expound the validation of ambipolarity of the radial particle transport. Taking equation (2), i.e. the perturbed density of electrons into the turbulent electron flux $\Gamma_e=\mathrm{Re}\left\langle \delta n_e \delta v_{\vec{E}\times\vec{B}}\right\rangle$, which is also divided into diffusive and convective parts, the normalized electron transport coefficients (normalization rule is similar with previous parts, i.e. $\hat{D}_e=\frac{D_e}{Rv_{thH}\left|\hat{\phi}_k\right|^2}$ and $\hat{V}_e=\frac{V_e}{v_{thH}\left|\hat{\phi}_k\right|^2}$) can be calculated,

$$\hat{D}_e=\sum_k\left[\begin{array}{l}\frac{\hat{\gamma}_k}{\hat{\omega}_r^2}\left(1+3G_{av}\tau_H k_y\rho_H\frac{1}{\hat{\omega}_r}\right)\\ +2\sqrt{\pi}\left(\frac{\hat{\omega}_r}{G_{av}\tau_H k_y\rho_H}\right)^{3/2}\exp\left(-\frac{\hat{\omega}_r}{G_{av}\tau_H k_y\rho_H}\right)\frac{1}{\hat{\omega}_r}\end{array}\right]\sqrt{2\varepsilon_0}(\tau_H k_y\rho_H)^2, \tag{16}$$

$$\hat{V}_e=\sum_k\left\{\begin{array}{l}\frac{3}{2}\frac{\hat{\gamma}_k}{\hat{\omega}_r^2}G_{av}\left(2\tau_H k_y\rho_H\frac{R}{L_{Te}}\frac{1}{\hat{\omega}_r}-1\right)-2\sqrt{\pi}\frac{1}{\tau_H k_y\rho_H}\left(\frac{\hat{\omega}_r}{G_{av}\tau_H k_y\rho_H}\right)^{3/2}\\ \times\exp\left(-\frac{\hat{\omega}_r}{G_{av}\tau_H k_y\rho_H}\right)\left[1+\frac{R}{L_{Te}}\left(\frac{3}{2}\tau_H k_y\rho_H\frac{1}{\hat{\omega}_r}-\frac{1}{G_{av}}\right)\right]\end{array}\right\}\sqrt{2\varepsilon_0}(\tau_H k_y\rho_H)^2, \tag{17}$$

with $b_H=k_y^2\rho_H^2$. Then, the validation of radial ambipolar relationship of turbulent fluxes $\Gamma_D+\Gamma_T+Z\Gamma_z=\Gamma_e$ requires the linear growth rate being

$$\hat{\gamma}_k^{amb}=\frac{2\sqrt{2\pi\varepsilon_0}\left(\frac{\hat{\omega}_r}{G_{av}\tau_H k_y\rho_H}\right)^{3/2}\exp\left(-\frac{\hat{\omega}_r}{G_{av}\tau_H k_y\rho_H}\right)\left[\hat{\omega}_r\left(\frac{R}{L_{Te}G_{av}}-1\right)+C_1\left(1-\frac{3}{2}\eta_e\right)\right]\hat{\omega}_r-\tau_H k_y\rho_H S l_0\tilde{f}_z\left(C_1\bar{K}+\hat{\omega}_r\right)}{C_1\left[1-\sqrt{2\varepsilon_0}\left(1-\frac{3}{2}\frac{G_{av}}{R/L_{ne}}\right)-\tau_H b_H\tilde{f}_z\bar{K}\right]-3\sqrt{2\varepsilon_0}\tau_H k_y\rho_H G_{av}K_e\frac{C_1}{\hat{\omega}_r}}. \tag{18}$$

Here, the term $3\sqrt{2\varepsilon_0}\tau_H k_y\rho_H G_{av}K_e\frac{C_1}{\hat{\omega}_r}$ in the denominator can be approximated as $3\sqrt{2\varepsilon_0}\tau_H k_y\rho_H G_{av}K_e$, if the higher order terms $\sim\mathrm{O}\left(\varepsilon_0^2\right)$ are neglected. Thus, the linear growth rate from the constraint of ambipolar turbulent flux is exactly the same as that from solving eigenvalue equation, i.e. equation (7). In other words, the ambipolarity of turbulent particle transport is self-consistently satisfied.

3.2. Parametric dependence of anomalous transport of helium ash, D and T ions

Based on the analytical results in section 3.1, we are going to study the parametric dependence of the anomalous transport of species α. As described in section 2, $\alpha=z$, D, T represents helium ash, D and T ions, respectively. The values of various parameters used in this subsection are the same as those in section 2.2 if there is no additional statement.

3.2.1. Effects of T_z and R/L_{nz}. Firstly, we study the dependence of the anomalous transport on the temperature of helium ash T_z (varying τ_z here actually means T_z is varying with fixed T_e=T_i). Figure 6(*a*) shows that the increase of τ_z brings a significant decrease in $\hat{D}_\alpha$, which is mainly due to the upshift of real frequency and the stabilization of instability resulting in the reduction of $\hat{D}_{\alpha 0}=\frac{\hat{\gamma}_k}{\hat{\omega}_r^2}$. For convective velocities in figure 6(*b*), both $\hat{V}_z$ and $\hat{V}_D$ are outward and decrease with increasing τ_z, while $\hat{V}_T$ increases from slightly inward to outward with the increase of τ_z. However, it is worth to notice that $\hat{D}_\alpha\gg\hat{V}_\alpha$, which means diffusion mechanism dominates over the convection. This is especially important for removing helium ash. Moreover, the difference between $\hat{D}_z$ and $\hat{D}_D$ is relatively small than that between $\hat{D}_z$ and $\hat{D}_T$. This is because the difference is resulted from FLR effects and acoustic terms. The good point is $\hat{D}_z$>$\hat{D}_T$ and the difference is slightly enhanced by lowering τ_z.

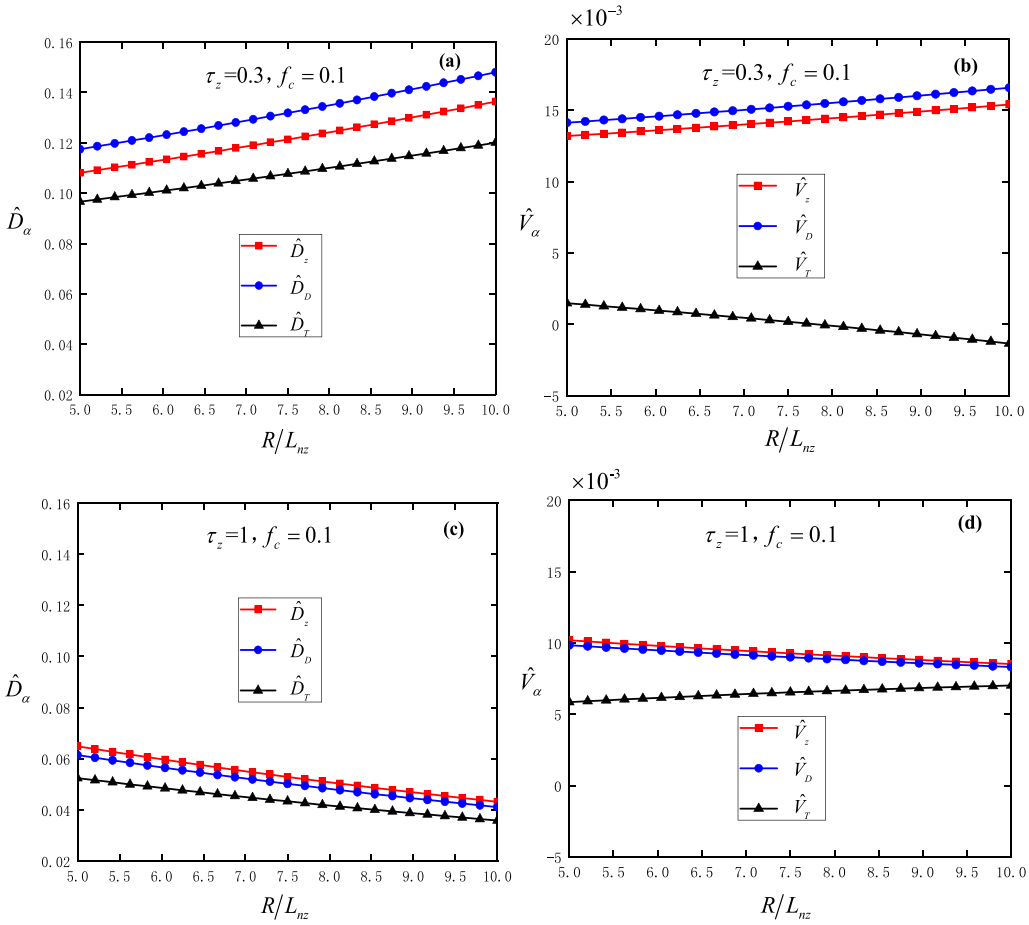

Figure 7. Transport coefficients of species α versus R/L_{nz}. τ_z= 0.3 in (*a*)–(*b*), while τ_z = 1 in (*c*)–(*d*).

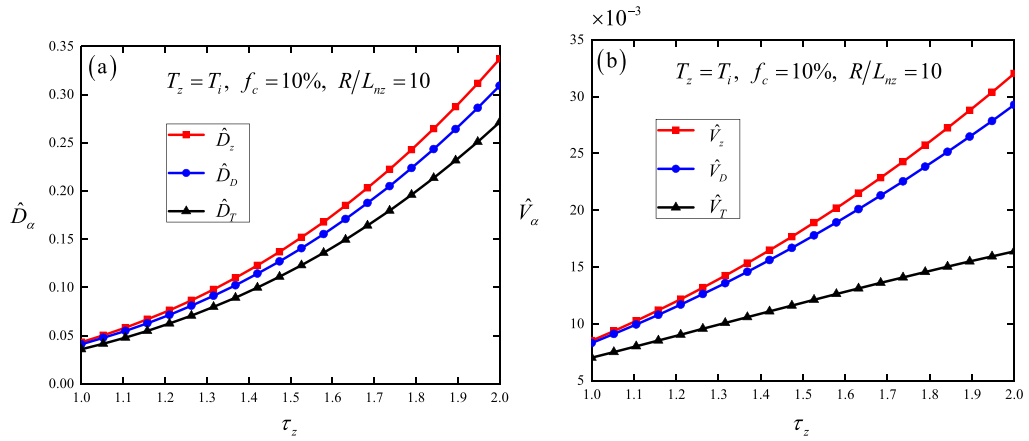

Figure 8. Transport coefficients of helium ash, D and T ions versus temperature ratio between electrons and helium ash τ_z. The increase of τ_z actually means T_e is increasing due to fixed $T_i = T_z$.

In section 2, it is found that when $\tau_z <$ (>) $\tau_{z,cri} = \tau_i \frac{A_z}{Z^2 A_{i,eff}} = 0.4$, increasing $R/L_{n\,z}$ destabilizes (stabilizes) CTEM instability. This indicates the effects of $R/L_{n\,z}$ on the associated anamolous transport of species α also depend on τ_z. Thus, we show how $R/L_{n\,z}$ affects the anomalous transport of helium, D and T ions for two cases in figure 7.

For the first (second) case with τ_z= 0.3 (τ_z= 1) in figures 7(*a*) (figure 7(*c*)), $\hat{D}_\alpha$ is increased (decreased) when we steepen the density profile of helium ash. This is again because the downshift (upshift) of $\hat{\omega}_r$ and the corresponding destabilization (stabilization) of $\hat{\gamma}_k$ (as shown in figure 3) by larger $R/L_{n\,z}$ increase (decrease) the lowest order of diffusivity

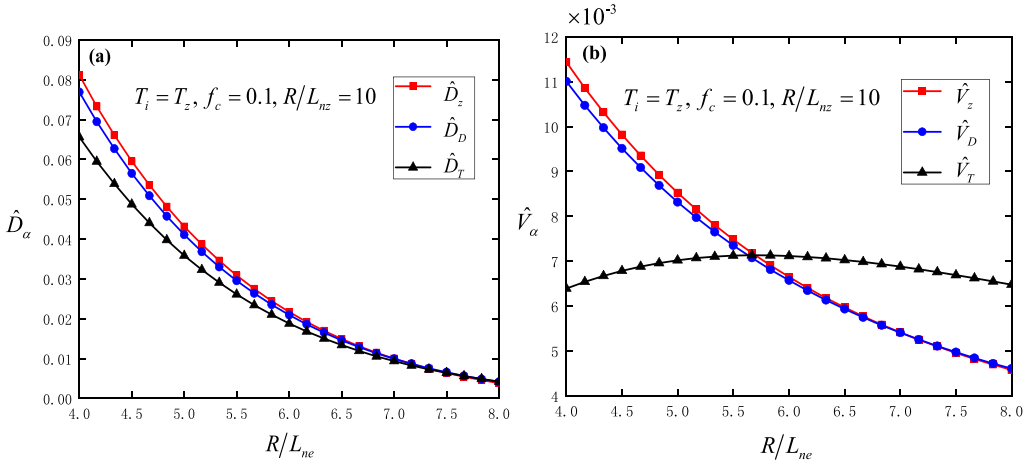

Figure 9. Transport coefficients of helium ash, D and T ions versus electron density profile R/L_{ne}.

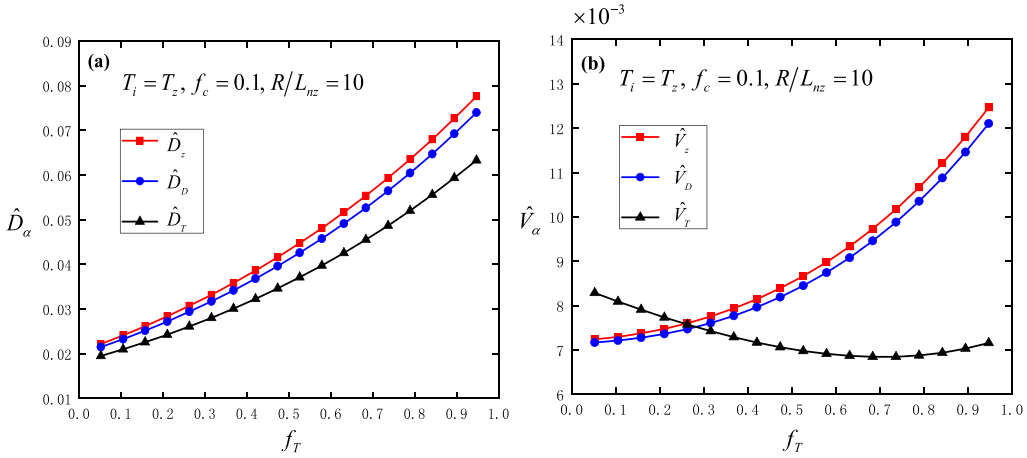

Figure 10. Transport coefficients of helium ash, D and T ions versus the fraction of T ions f_T.

$\hat{D}_{\alpha 0} = \frac{\hat{\gamma}_k}{\hat{\omega}_r^2}$. Although outward $\hat{V}_T$ in figure 7(b) decreases and even changes into inward and $\hat{V}_z$ and $\hat{V}_D$ increase with the increase of $R/L_{n\,z}$, the convection is still much smaller than diffusion as mentioned above. Moreover, the trend of $\hat{D}_D > \hat{D}_z > \hat{D}_T$ ($\hat{D}_z > \hat{D}_D > \hat{D}_T$) in figure 7($a$) (figure 7($c$)) is slightly strengthened by larger (smaller) $R/L_{n\,z}$.

From figures 6 and 7, we conclude that the diffusivity dominants over convection. This is favourable for exhausting helium ash especially when its temperature is slightly higher than that of background plasmas. Moreover, higher transport level of helium ash than that of T ions can be achieved for a wide parameter regime for the density profile of helium ash. But, the diffusivity of helium ash can be either greater or smaller than that of D ions, which depends on the temperature ratio of electron (ion) to helium ash.

3.2.2. Effects of T_e and R/L_{ne}. Similar to figure 4, increase of τ_z here actually means T_e becomes larger due to fixed T_i=T_z. Figure 8 clearly demonstrates that the increase of T_e significantly enhances the diffusivity $\hat{D}_\alpha$ and it satisfies $\hat{D}_z > \hat{D}_D > \hat{D}_T$ and $\hat{V}_z > \hat{V}_D > \hat{V}_T > 0$ as shown in figures 8(a) and (b), respectively. Enhanced anomalous diffusivity of helium ash here due to the increase of T_e is qualitatively consistent with the prediction given by GKW in [8]. Besides, figure 8(a) also shows that the larger τ_z it is, the more significant difference between $\hat{D}_z$ and $\hat{D}_i$ as well as between $\hat{V}_z$ and $\hat{V}_i$ we have.

Meanwhile, it reveals that the diffusivities of helium ash, D and T ions in figure 9(a) as well as the outward $\hat{V}_z$ and $\hat{V}_D$ in figure 9(b) are all enhanced by decreasing R/L_{ne} (i.e. flattening the electron density profile) as demonstrated in equations (14) and (15). But, for T ions, $\hat{V}_T$ does not change too much with R/L_{ne}. Since convective part is still much weaker than diffusive part, the key point here is that the diffusivity of helium is enhanced more than that of D-T ions by flattening the electron density profile.

Incorporating the results in figures 8 and 9, we may conclude that flattening the electron density profile and increasing T_e are favorable for expelling helium ash through CTEM turbulence. The exhaust of argon in the ECRH heated plasmas (with increase of T_e and flattening of electron density) has been observed in high β_p mode plasma of JT-60U [14],

Table 1. Parametric dependence of CTEM instability in D-T plasmas with helium ash.

Increasing parameter	$\hat{\omega}_r$		$\hat{\gamma}_k$	
f_c R/L_{nz}	τ_z<0.4: downshift	τ_z>0.4: upshift	τ_z<0.4: destabilize	τ_z>0.4: stabilize
T_z	Downshift		Destabilize	
T_e	Upshift		Destabilize	
R/L_{ne}	Upshift		Stabilize	
f_T	Downshift		Destabilize	

Table 2. Parameter regime favorable for expelling more helium ash than D and T ions through CTEM turbulence.

Trend	Variation of parameters to enhance the trend
$\hat{D}_D>\hat{D}_z>\hat{D}_T$	Higher T_z and larger R/L_{nz}
$\hat{D}_z>\hat{D}_D>\hat{D}_T$	Smaller R/L_{nz} Higher T_e Smaller R/L_{ne} Larger f_T

although it is attributed to the reduction of the neoclassical inward convection velocity. It would be very interesting to test ECRH effects on helium transport in similar condition.

3.2.3. Isotopic effects. Last but not the least, we study the isotopic effects by varying the fraction of T ions f_T. As shown in figure 10(*a*), more T ions in D-T plasmas clearly enhances $\hat{D}_\alpha$, which is mainly due to the enhanced $\hat{D}_{\alpha 0}$ by stronger FLR effects on instability as explained before. Moreover, the trend for $\hat{D}_z>\hat{D}_D>\hat{D}_T$ is further strengthened by increasing the fraction of T ions. Again, the convection is much smaller than the diffusion. It indicates that the isotopic effects may also help remove more helium ash than D-T ions.

4. Summary

In the present work, we have investigated the anomalous transport of helium ash, D and T ions driven by CTEM turbulence under weak magnetic regime. The eigenvalues of CTEM instability are derived and the parametric dependence of CTEM instability with helium ash is studied. Moreover, the quasi-linear turbulent fluxes of helium ash, D and T ions are calculated and divided into diffusion and convection parts. Then, the detailed parametric dependence of the anomalous transport of helium ash, D and T ions is studied in order to find parameter regime to exhaust more helium ash than D-T ions. The main results can be found in tables 1 and 2.

It needs to be stressed that, under the parameter used in this paper, we find $\hat{D}_\alpha \gg \hat{V}_\alpha$, and thus just list how to enhance the difference between $\hat{D}_z$ and $\hat{D}_i$ in table 2. The main conclusions are worth to be stressed again as

(a) The diffusivity dominates over convection, which is favorable for exhausting helium ash especially when its temperature is slightly higher than that of background plasmas;

(b) The trend of expelling more helium ash than D-T ions is evidently strengthened by increasing T_e and flattening electron density profile as well as increasing f_T.

It would be interesting to test our theoretical results by gyrokinetic simulation, and explore the nonlinear process, which may bring new physics in the burning plasmas. Extension of this work to predict helium ash profile by including helium ash source is worth of exploring in the future. Because the energetic alpha particles mainly heat electrons, the electron temperature gradient driven CTEM turbulence could be another important candidate for helium ash transport. It may also need considering the other type of microturbulence driven anomalous transport or even neoclassical transport in the very central region, where helium ash is produced. This is because CTEM turbulence may not be dominant mechanism for helium transport due to small fraction of trapped electrons in the very central region. There are also many other interesting related works left for future. For example, it is found that resonant magnetic perturbation (RMP) decreases the confinement time of helium impurity [56], and the removal of helium ash is also identified by ICRH-driven ripple transport [57]. However, the physical mechanism about why those non-axisymmetric perturbed magnetic field helps expel helium ash is not very clear, and it is worth to explore. Electromagnetic (EM) effects on impurity transport have attracted attention [44, 58]. Therefore, studying the helium ash transport driven by EM turbulence such as kinetic ballooning mode (KBM) turbulence in the future is of great significance. Besides, the TEM turbulence is also found to evidently influence the transport of other impurities [59] such as tungsten (W) [60, 61], which is another important impurity in ITER. Our ongoing work is to investigate how ECRH affects the transport of W in the D-T plasmas.

Acknowledgments

The authors are grateful to Professor P. H. Diamond for lots of discussions during the implement of this work. We also acknowledge Professors K. Ida, Vincent Chan for useful and interesting discussions. This work was supported by the National Key R&D Program of China under Grant Nos. 2017YFE0302000 and 2017YFE0300501, the National Natural Science Foundation of China under Grant Nos.11905079 and 11675059, and by the Initiative Postdocs Supporting Program of China under Grant No. BX20180105, National Natural Science Foundation of China under Grant No. 51821005.

ORCID iDs

Weixin Guo https://orcid.org/0000-0001-7677-799X
Lu Wang https://orcid.org/0000-0002-5881-6139

References

[1] ITER Physics Basis 1999 Chapter 2: plasma confinement and transport *Nucl. Fusion* **39** 2175
[2] Redi M.H., Cohen S.A. and Synakowski E.J. 1991 *Nucl. Fusion* **31** 1689
[3] Nakamura H. *et al* 1991 *Phys. Rev. Lett.* **67** 2658
[4] Zastrow K.D. *et al* 2005 *Nucl. Fusion* **45** 163
[5] Hogan J. 1997 *J. Nucl. Mater.* **241–243** 68
[6] Hogan J. and Hillis D. 2000 *Nucl. Fusion* **40** 879
[7] Ida K., Yoshinuma M., Goto M., Schmitz O., Dai S., Bader A., Kobayashi M., Kawamura G., Moon C. and Nakamura Y. 2016 *Plasma Phys. Controlled Fusion* **58** 074010
[8] Kappatou A. *et al* 2019 *Nucl. Fusion* **59** 056014
[9] Fonck R.J. and Hulse R.A. 1984 *Phys. Rev. Lett.* **52** 530
[10] Synakowski E.J., Stratton B.C., Efthimion P.C., Fonck R.J., Hulse R.A., Johnson D.W., Mansfield D.K., Park H., Scott S.D. and Taylor G. 1990 *Phys. Rev. Lett.* **65** 2255
[11] Synakowski E.J. *et al* 1993 *Phys. Fluids* B **5** 2215
[12] Hillis D.L. *et al* 1990 *Phys. Rev. Lett.* **65** 2382
[13] Wade M.R. *et al* 1995 *Phys. Plasmas* **2** 2357
[14] Takenaga H. *et al* 2003 *Nucl. Fusion* **43** 1235
[15] Horton W. 1999 *Rev. Mod. Phys.* **71** 735
[16] Synakowski E.J. *et al* 1995 *Phys. Rev. Lett.* **75** 3689
[17] Angioni C., Peeters A.G., Pereverzev G.V., Bottino A., Candy J., Dux R., Fable E., Hein T. and Waltz R.E. 2009 *Nucl. Fusion* **49** 055013
[18] Guo W., Wang L. and Zhuang G. 2016 *Phys. Plasmas* **23** 112301
[19] Guo W., Wang L. and Zhuang G. 2019 *Nucl. Fusion* **59** 076012
[20] D'Angelo N. 1965 *Phys. Fluids* **8** 1748
[21] Catto P.J. 1973 *Phys. Fluids* **16** 1719
[22] Adam J.C., Tang W.M. and Rutherford P.H. 1976 *Phys. Fluids* **19** 561
[23] Henderson S.S., Garzotti L., Casson F.J., Dickinson D., Fox M.F.J., O'Mullane M., Patel A., Roach C.M., Summers H.P. and Valovič M. 2014 *Nucl. Fusion* **54** 093013
[24] Angioni C. and Peeters A.G. 2006 *Phys. Rev. Lett.* **96** 095003
[25] Ida K. *et al* 2018 Isotope effect on impurity and bulk ion particle transport in the Large Helical Device *Preprint: 2018 IAEA Fusion Energy Conf.* (Gandhinagar, India, 22–27 October 2018) [EX/10-1] (https://www.iaea.org/sites/default/files/18/10/cn-258-programme.pdf)
[26] Efthimion P.C. *et al* 1995 *Phys. Rev. Lett.* **75** 85
[27] Neverov V.S., Kukushkin A.B., Kruezi U., Stamp M.F. and Weisen H. 2019 *Nucl. Fusion* **59** 046011
[28] Nakata M., Nagaoka K., Tanaka K., Takahashi H., Nunami M., Satake S., Yokoyama M. and Warmer F. 2019 *Plasma Phys. Controlled Fusion* **61** 014016
[29] Yamada H. *et al* 2019 *Phys. Rev. Lett.* **123** 185001
[30] Ida K., Nakata M., Tanaka K., Yoshinuma M., Fujiwara Y., Sakamoto R., Motojima G., Masuzaki S., Kobayashi T. and Yamasaki K. 2020 *Phys. Rev. Lett.* **124** 025002
[31] Garcia J., Görler T., Jenko F. and Giruzzi G. 2017 *Nucl. Fusion* **57** 014007
[32] Bonanomi N., Angioni C., Crandall P.C., Di Siena A., Maggi C.F. and Schneider P.A. 2019 *Nucl. Fusion* **59** 126025
[33] Nakata M., Nunami M., Sugama H. and Watanabe T.H. 2017 *Phys. Rev. Lett.* **118** 165002
[34] Belli E.A., Candy J. and Waltz R.E. 2019 *Phys. Plasmas* **26** 082305
[35] Bustos A., Bañón Navarro A., Görler T., Jenko F. and Hidalgo C. 2015 *Phys. Plasmas* **22** 012305
[36] Takeiri Y. 2018 *IEEE Trans. Plasma Sci.* **46** 1141
[37] Takahashi H. *et al* 2018 *Nucl. Fusion* **58** 106028
[38] Joffrin E. *et al* 2019 *Nucl. Fusion* **59** 112021
[39] Nakata M., Nunami M., Sugama H. and Watanabe T.H. 2016 *Plasma Phys. Controlled Fusion* **58** 074008
[40] Shen Y., Dong J.Q., Sun A.P., Qu H.P., Lu G.M., He Z.X., He H.D. and Wang L.F. 2016 *Plasma Phys. Controlled Fusion* **58** 045028
[41] Guo W., Wang L. and Zhuang G. 2017 *Nucl. Fusion* **57** 126052
[42] Li J. and Kishimoto Y. 2002 *Plasma Phys. Controlled Fusion* **44** A479
[43] Dong J.Q. 2018 *Plasma Sci. Technol.* **20** 094005
[44] Hein T. and Angioni C. 2010 *Phys. Plasmas* **17** 012307
[45] Du H., Wang Z.X. and Dong J.Q. 2016 *Phys. Plasmas* **23** 072106
[46] Rewoldt G., Tang W.M. and Frieman E.A. 1980 *Phys. Fluids* **23** 2011
[47] Dominguez R. and Staebler G. 1993 *Nucl. Fusion* **33** 51
[48] Idouakass M., Gravier E., Lesur M., Médina J., Réveillé T., Drouot T., Garbet X. and Sarazin Y. 2018 *Phys. Plasmas* **25** 062307
[49] Dux R., Neu R., Peeters A.G., Pereverzev G., M Ck A., Ryter F., Stober J. and Team A.U. 2003 *Plasma Phys. Controlled Fusion* **45** 1815
[50] Gohil P. *et al* 2003 *Plasma Phys. Controlled Fusion* **45** 601
[51] Hong J. *et al* 2017 *Nucl. Fusion* **57** 036028
[52] Hong J. *et al* 2015 *Nucl. Fusion* **55** 063016
[53] McDermott R.M., Angioni C., Dux R., Fable E., Pütterich T., Ryter F., Salmi A., Tala T., Tardini G. and Viezzer E. 2011 *Plasma Phys. Controlled Fusion* **53** 124013
[54] Sommer F. *et al* 2012 *Nucl. Fusion* **52** 114018
[55] Shen Y., Dong J.Q., Han M.K., Sun A.P. and Shi Z.B. 2018 *Nucl. Fusion* **58** 076007
[56] Schmitz O. *et al* 2016 *Nucl. Fusion* **56** 106011
[57] Hamamatsu K., Chang C.S., Takizuka T., Azumi M., Hirayama T., Cohen S. and Tani T. 1998 *Plasma Phys. Controlled Fusion* **40** 255
[58] Petty C.C. *et al* 2004 *Phys. Plasmas* **11** 2514
[59] Gravier E., Lesur M., Garbet X., Sarazin Y., Médina J., Lim K. and Idouakass M. 2019 *Phys. Plasmas* **26** 082306
[60] Angioni C., Bilato R., Casson F.J., Fable E., Mantica P., Odstrcil T. and Valisa M. 2017 *Nucl. Fusion* **57** 022009
[61] Lesur M. *et al* 2020 *Nucl. Fusion* **60** 036016